Hindawi
Wireless Communications and Mobile Computing
Volume 2018, Article ID 9163783, 15 pages
https://doi.org/10.1155/2018/9163783

*Research Article*

# Impact of Resource Blocks Allocation Strategies on Downlink Interference and SIR Distributions in LTE Networks: A Stochastic Geometry Approach

**Anthony Busson**[1] **and Iyad Lahsen-Cherif**[2]

[1]*INRIA CNRS UMR 5668 LIP, University Lyon 1, France*
[2]*CNRS UMR 8623 LRI, University Paris Saclay, France*

Correspondence should be addressed to Anthony Busson; anthony.busson@inria.fr

Received 26 January 2018; Revised 5 May 2018; Accepted 28 May 2018; Published 26 June 2018

Academic Editor: Natalia Y. Ermolova



We propose a model based on stochastic geometry to assess downlink interference and signal over interference ratio (SIR) in LTE networks. The originality of this work lies in the proposition and combination of resource blocks assignment strategies, transmission power control, and realistic traffic patterns into a stochastic geometry model. For this model, we compute the first two moments of interference. They are used to parameterize its distribution from which we deduce the SIR distribution. Outage and transmission rates (modulation and coding rate) are then derived to evaluate the system performance. Simulations that cover a large set of scenarios show the accuracy of our proposal and allow us to compare these strategies with more complex ones that aim to minimize global interference. Numerical evaluations highlight the behavior of the LTE network for different traffic patterns/load, eNodeB density, and amount of resource blocks and offer insights about possible parameterization of LTE networks.

## 1. Introduction

The amount of mobile data that cellular networks must carry is continuously increasing. The capacity of the wireless systems must continuously increase in order to satisfy the growing demand of traffic from users and applications. Long-Term Evolution and Long-Term Evolution-Advanced [1] (LTE-A) have been recently standardized to improve the network capacity and support this traffic growth. One of the solutions brought by LTE is the enhancement of the radio spectrum reuse. The smallest radio resource that can be allocated to a user is a *resource block* (RB). An RB is a channel (an OFDMA channel composed of a set of OFDM subcarriers) for the duration of one time slot. Considering the number of RB is finite, they are reused in different cells generating potential intercell interference. The algorithms that assign RB to users located in different cells have thus an important role in the system performance. A static RB assignment where disjoint resources are distributed to each cell may lead to an inefficient resource usage as the unused RB in a cell cannot be reused in another one. Instead, algorithms that assign RB can be centralized in a scheduler/controller that controls a certain number of neighborhood cells and adapts the RB assignments to the cells load. Also, it may improve the spatial reuse while ensuring a low level of interference.

Several studies have proposed assignment strategies performed at the scheduler to minimize global interference [2, 3]. These strategies aim to minimize interference for a given configuration and are evaluated exclusively through simulations. However, the assignment strategies have to be evaluated for more general scenarios and at larger scale.

Stochastic geometry offers a powerful tool to analyze large scale networks through a few parameters and to understand the role of these key parameters on the whole system. The other benefit of stochastic geometry is to consider realistic Base stations (BS) or eNodeB (*evolved Node B*) locations. It uses random point processes rather than deterministic (grid or hexagonal patterns for instance) or predetermined locations of BS/eNodeB. For instance, the Poisson Point

Process (PPP) has been shown to be suitable to model the spatial location of BS [4–6]. Nevertheless, interference as experienced by a user is not generated by all BS but only by the ones using the same radio resources. The resource allocation strategies have thus to be mapped to the point process modeling BS/eNodeB to determine which points/BS are interfering with a given communication. Consequently, the traffic demand must also be taken into account as it sets the number of resources used at a given time.

In this work, we propound a combination of several assignment strategies, realistic traffic demands, and transmission power control mechanisms into a stochastic geometry model. We begin by reviewing related works and our contributions.

*1.1. Related Work.* In a downlink LTE system, a resource block (RB) is the smallest radio resource unit that can be allocated to a user. The LTE system has to schedule and assign RB to users as a function of the link qualities, traffic demands, and potential quality of service requirements. In this paper, we focus on a system where a controller assigns RB for a set of eNodeB. We do not overview RB assignment techniques in LTE network as they aim to optimize RB assignments and modulation/coding rates for a given topology and a traffic demand. Instead, this paper deals with the macroscopic design of the network: the impact of eNodeB density, allocation scheme, and power allocation on the global performance of a downlink LTE system. Nevertheless, the reader can refer to [7, 8] for recent surveys. Also, interesting contributions on the optimization of the downlink system for a given configuration are described in [3, 9–12].

Stochastic geometry has emerged as an efficient tool to analyze the performance of cellular networks. It offers, through simple models, a way to study wireless architectures at a large scale. Recent surveys [13, 14] summarize the numerous wireless architectures and models for which stochastic geometry has been applied. One of the main difficulties in the analysis of large wireless systems is to characterize interference. This quantity does not depend only on BS location and radio environment (path loss, shadowing/fading, etc.), but also on the way that radio resources (time, frequency, and power) are allocated. The point process modeling interfering nodes is thus of crucial importance. The PPP offers an accurate model to describe BS location [4–6]. This process is tractable, and it is possible to derive closed formulas for some key performance metrics of the system: interference, coverage, outage, Signal over Interference plus Noise Ratio (SINR), etc. But the PPP models all BS/eNodeB and not the subset of interfering eNodeB for a given communication. The process has thus to be thinned to take into account interference coordination (IC) techniques and radio resources assignment, for example, leading to processes that are no more Poisson. In the next paragraph, we focus on recent contributions, and on studies where resources allocation and more generally IC techniques are taken into account.

IC refers to techniques that aim to mitigate interference at the receivers. Surveys on such techniques can be found in [2, 15]. A common IC approach consists in controlling the allocated radio resources (frequency/time/power) in order to alleviate the interference impact on communications. In [16], the authors consider a random resources allocation strategy where the BS are distributed as a PPP. This simple and tractable strategy allows model interfering BS as an independent thinning of a PPP and deriving closed formulas for the coverage probability. They also deduce the minimal reuse factor achieving a given coverage probability. The performance of strict FFR (Fractional Frequency Reuse) and SFR (Soft FFR) allocation strategies is evaluated using stochastic geometry in [17]. With these two techniques, different radio resources are allocated to users that are at the edge of a cell (Voronoï cells here) with regard to the ones close to the BS. The criteria distinguishing core and edge users is based on the SINR at each user computed from the underlying PPP modeling all BS. For strict FFR, the radio resources used at the edge and in the core are disjoint. Instead, the radio resources may be reused between the two regions for SFR. For these two strategies, the authors derive closed formulas for the coverage probability and discuss pros and cons of these approaches. A superior interference reduction is observed for FFR but SFR benefits from a greater resource efficiency. This work is generalized in [18, 19] to the context of K-tier and heterogeneous networks considering different point processes for each tier or network technology. It is also extended and studied in [20] with the dynamic strict FFR (DSFFR) where the edges of the cells are dynamically divided into sectors with the help of directional antennas. In [21], a coordinated beamforming is employed to ensure that a set of closed BS, "a cluster", will use different resources. A user associated with a BS is then not subject to interference from BS belonging to the same cluster. The authors derive analytical expressions for the Signal over Interference Ratio (SIR) for this strategy and discuss the impact of the clusters cardinality. A similar approach is used in [22], where the set of coordinated BS corresponds to the most interfering ones. Interference level takes into account path loss and long-term shadowing. The interfering BS are outside this set. They are selected randomly and independently leading to a thinned PPP. For this model, the authors study the coverage probability for different scenarios. In [23], a user is served by its 1 or 2-closest BS according to the position of these BS with regard to the user. When the two BS are coordinated, the transmission power is split into the two transmissions. The total transmission power is thus the same with one or two coordinated BS. Interference is generated by the other BS without restriction which is assumed to be distributed through a PPP. The authors derive a closed-form expression for the SIR distribution and the network coverage probability and discuss the benefit of this approach. In [24], an IC technique is evaluated for a user at the edge of its cell. When the resource of this communication is used by neighboring cells, they may not transmit any signal for a certain period to mitigate interference at this user. This coordination technique is analytically evaluated assuming that interfering nodes are still distributed as a PPP.

Besides the modeling of IC, [22, 25–27] propose spatial and tractable models that take into account the traffic demand in the interference computation, but they do not consider

concrete RB assignment algorithms. In particular, the authors in [26] study SIR coverage for a cellular network based on PPP. A queue is associated with each BS that determines the BS transmission activity as a function of the traffic. Considering the traffic at each BS is independent, interferers at a given time are then an independent thinning of the initial PPP and are still Poisson. This model differs with this paper as we do not take into account eNodeB activity as a function of the traffic but instead the resource allocation as a function of the number of associated users to each eNodeB. Also, stochastic geometry models can be specific to certain power control scheme [28] or radio technologies as in [29] where the authors consider a K-tier heterogeneous network with transmissions operating on the millimeter wave band.

*1.2. Contributions.* The primary contribution of this work is to offer an analytical model based on stochastic geometry to evaluate the performance of a downlink LTE system taking into account RB allocation strategies, power control, and traffic demands. All these mechanisms have never been combined into a single stochastic geometry model. The number of allocated resources for an eNodeB is assumed to follow the distribution of the number of clients in an M/M/C/C queue. It models the number of communications in progress when both the interarrival of the communications and their duration follow an exponential distribution. Such assumptions are pertinent in cellular networks as it has been recently shown in [30]. We associate to these traffic demands several resource allocation strategies. All these algorithms are combined with a power control mechanism that depends on the channels quality. Allocation strategies lead to non-PPP as correlation appears between the locations of the interfering nodes. It prevents the use of the convenient properties of the PPP to compute interference distribution. Nevertheless, we propose approximations that allow us to deal with these correlations and to obtain an analytical method that is shown very accurate with regard to simulations.

We compare our model to classical optimization approaches where, for a given configuration/sample, the allocation is optimized with regard to an objective function. To our knowledge, such comparison has never been done before. It shows that geometry stochastic based model may be relevant to offer tight approximations on wireless system performance.

Models are evaluated through a large set of simulations that highlights benefits of our approach to design some key parameters of the wireless system. Results show that the obtained values for SIR, coding, and modulation rates correspond to the reference values of the standards and technical LTE documents, empirically proving that our model is able to approximate performance of real systems. This work has been partially presented in [31].

*1.3. Paper Organization.* The remainder of this work is organized as follows. In the next section we present the system model. We expose the assignment strategies in Section 3. In Section 4, we derive the first and second moments of interference for each allocation strategy. SIR distribution is assessed in Section 5. Numerical results and simulations are presented and discussed in Section 6. We conclude the paper in Section 7.

## 2. System Model

*2.1. eNodeB Location and Interference.* eNodeB location is modeled by a point process $N_e = \{X_i\}_{i\in\mathbb{N}}$ distributed in $\mathbb{R}^2$ with intensity $\lambda_e$. Its distribution is detailed in Section 2.2. The eNodeB are numbered with regard to their distance to the origin, eNodeB 0 at $X_0$ being the closest one. We consider a downlink system between a typical user and its attached eNodeB. Without loss of generality, we assume that this user is located at the origin. The users are assumed to be associated with their closest eNodeB with regard to the Euclidean distance. The channels between eNodeB and the typical user are modeled through a sequence of i.i.d. random variables $(h_i)_{i\in\mathbb{N}}$. The transmission power between an eNodeB and one associated user is given by the function $T_x(r)$. This function models the power control algorithm implemented by the eNodeB and depends on the distance $r$ between a user and its attached eNodeB. The scheduler/controller manages a set of $RB_{max}$ resource blocks that are common to all eNodeB. They are thus shared between eNodeB. The RB are numbered from 0 to $RB_{max} - 1$. The scheduler assigns one RB for each user, but the model can be easily extended with a random number of RB for each demand. Traffic demands exceeding $RB_{max}$ at an eNodeB are not served. The RB with index 0 is allocated to the typical user. We show, in the appendix, that this choice does not impact the computations, and any other index could be chosen instead. An eNodeB interferes with the typical user if and only if it reuses this RB. Interference at the typical user can be expressed as

$$I\left(\|X_0\|\right) = \sum_{i=1}^{\infty} w_i \cdot h_i \cdot T_x\left(\|X_i - U_i\|\right) \cdot l\left(\|X_i\|\right), \qquad (1)$$

where $l(\cdot)$ is the path loss function. The argument of interference is the distance between the typical user and its eNodeB (eNodeB 0). $I(\|X_0\|)$ expresses interference when this distance is random and depends on the r.v. $\|X_0\|$. $I(r)$ expresses interference when this distance is given and equal to $r$. This notation is motivated by the fact that the r.v. $X_i$ and $X_i - U_i$ are correlated to $X_0$. Moreover, the mean and the variance of interference will be computed for both a given value of $\|X_0\|$ and with regard to its distribution. The r.v. $w_i$ indicates whether eNodeB $i$ interferes with the typical user ($w_i = 0$ or 1). $U_i$ is the random variable modeling the location of a user attached to the eNodeB $i$ (at $X_i$). We assume that $U_i$ is uniformly distributed in the Voronoï cell formed by the process $N_e$ and with nucleus $X_i$. The main notations used throughout this paper are given in Table 1.

*2.2. Point Process Modeling eNodeB.* The point process modeling eNodeB is a modified homogeneous PPP. The process $N_e \setminus \{X_0\} = \{X_i\}_{i>0}$ is Poisson in $\mathbb{R}^2 \setminus B(0, \|X_0\|)$ where $B(0, \|X_0\|)$ is the ball centered at the origin and with radius $\|X_0\|$. We choose a distribution for $\|X_0\|$ that makes the process $N_e$ different of a PPP. Indeed, with a PPP the typical user at the origin lies in a Voronoï cell that is greater in

Table 1: Principal notation.

| | |
|---|---|
| $N_e$ | point process modeling eNodeB |
| $I(\|X_0\|)$ | interference at the typical user. The distance between the typical user and eNodeB 0 is the r.v. $\|X_0\|$. |
| $I(r)$ | interference at the typical user. The distance between the typical user and eNodeB 0 is equal to $r$. |
| $w_i$ | r.v. indicating if eNodeB $i$ interferes with the typical user |
| $D_i$ | number of RB allocated to eNodeB $i$ |
| $T_x(r)$ | transmission power between an eNodeB and its user at distance $r$ |
| $\Delta$ | spatial reuse parameter (an RB is reused every $\Delta$ eNodeB in average) |
| $f_{\|X_i\|}(\cdot)$ | PDF of $\|X_i\|$ |
| $f_{\|X_i\|,\|X_j\|}(\cdot,\cdot)$ | joint PDF of $(\|X_i\|, \|X_j\|)$ |
| $f^i_{\|X_0\|=r}(\cdot)$ | conditional PDF of $\|X_i\|$ given that $\|X_0\| = r$ |
| $f^{i,j}_{\|X_0\|=r}(\cdot)$ | conditional PDF of $(\|X_i\|, \|X_j\|)$ given that $\|X_0\| = r$ |
| $f^0_{\|X_0\|}(\cdot)$ | PDF of the distance between the typical user (at the origin) and its serving eNodeB 0 |
| $f^0_{\|U_i-X_i\|}(\cdot,\cdot)$ | conditional PDF of the distance between a user and its attached nucleus $X_i$ given $\|X_i\|$ |

average than the other cells. Intuitively, "big cells" cover more space than "small cells" and consequently the cell covering the origin has a greater size in average. It is consistent with a modeling where users are homogeneously scattered in the plane but not with our assumption where the network has been dimensioned to have the same load in average (the same number of users) in each cell. It is more realistic as it has been shown in [30], where a homogeneous load is observed for the different cells independently of their sizes. In this case, the typical cell covering the typical user must have the same distribution as the other cells. Therefore, we consider the distribution of the distance $\|X_0\|$ under Palm measure. More precisely, this distribution corresponds to the distance between the nucleus of a typical cell under Palm measure and a point uniformly distributed in this cell. The distribution of this distance is not known, but we use the approximation presented in [32] (page 133). We set the distribution of the distance between the typical user and its closest eNodeB at $X_0$ as

$$f^0_{\|X_0\|}(r) = 2\pi\lambda_e c r e^{-\lambda_e c \pi r^2} \tag{2}$$

with $c = 1.25$. The angle between the lines $(0, X_0)$ and the abscissa is uniformly distributed in $[0, 2\pi)$.

The distribution of the distance between a user in a given Voronoï cell and its nucleus $(\|X_i - U_i\|)$ follows the same definition, and consequently the same distribution. In the next section, we present the different RB assignment strategies evaluated in this paper.

## 3. Assignment Strategies

We consider four different allocation strategies. We begin by two simple RB allocation schemes: independent and static allocations. Then, we develop a more realistic allocation strategy using the $M/M/RB_{max}/RB_{max}$ queue, named $M/M/RB_{max}/RB_{max}$ allocation hereafter. Also, a more global approach where the RB are assigned in order to minimize the sum of interference at each user is considered but for which we do not propose a mathematical resolution. All the allocation strategies are set in such a way that a given RB is reused every $\Delta$ ($\Delta \geq 1$) eNodeB in average. The mean load in each cell and equivalently the mean number of RB used by an eNodeB are then $RB_{max}/\Delta$. The reuse factor $\Delta$ reflects the network load.

*3.1. Independent Allocation: Thinning.* With this strategy, each eNodeB selects its resources independently of the other eNodeB. Therefore, we assume that an eNodeB has a probability $1/\Delta$ to reuse the RB with index 0. The point process describing the interfering eNodeB is then a thinned PPP in $\mathbb{R}^2 \setminus B(O, \|X_0\|)$ with intensity $\lambda_e/\Delta$.

*3.2. Static Allocation.* We assign a constant proportion $RB_{max}/\Delta$ of the available resources to each eNodeB. They are allocated in their index order: eNodeB 0 uses RB from 0 to $RB_{max}/\Delta - 1$ (it includes the typical user), eNodeB 1 from $RB_{max}/\Delta$ to $2(RB_{max}/\Delta) - 1$, etc. We take the integer part of these fractions when $RB_{max}$ is not a multiple of $\Delta$. We loop when all resources have been used. Consequently, the eNodeB interfering with the typical user has an index with the form $k \cdot \Delta$ with $k > 0$.

*3.3. $M/M/RB_{max}/RB_{max}$ Allocation.* In an $M/M/C/C$ queue, customers arrive according to a Poisson process (in $\mathbb{R}$) and the service times are exponentially distributed. It models a system with $C$ resources/servers and a capacity of the same size. A customer cannot enter in the system if all resources/servers are busy. We associate with each eNodeB an independent $M/M/RB_{max}/RB_{max}$ queue to model the number of RB in use. The servers model the RB. Upon the arrival of a request/user, an RB/server is used for a time exponentially distributed. If no RB is available, the request is rejected. In order to have a mean reuse factor of $\Delta$, the parameter of the queue (the load) denoted $\rho$ is set in such a way that the mean number of customers in the system, or equivalently the mean number of busy resource blocks, is equal to $RB_{max}/\Delta$. The distribution of the number of busy

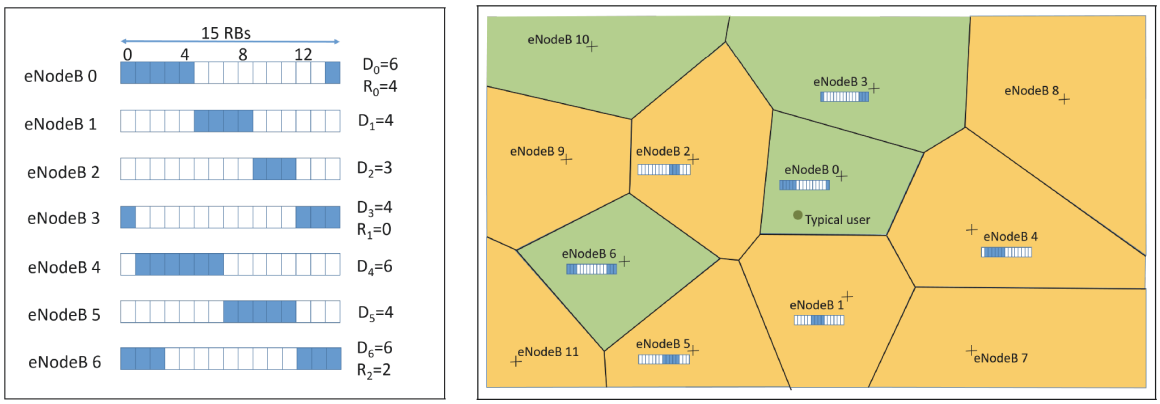


(a) RB allocation

(b) Impact of RB allocation on interferer

Figure 1: In Figure 1(a) an example of RB allocation is given. eNodeB 0 uses 6 RB (the first one has index 14, and the other ones are indexed from 0 to 4). It uses the RB with index 0 to communicate with the typical user. $R_0$ is the index of the last resource used by eNodeB 0. As it uses RB indexed from 14 to 4, $R_0 = 4$ here. The number of used RB for the other eNodeB are $D_1 = 4$, $D_2 = 3$, etc. An eNodeB interferes if and only if it reuses the resource 0: in this example eNodeB 3 and 6. In Figure 1(b), we plot a sample of the point process describing eNodeB location with the same RB assignment. The eNodeB interfering with the typical user is then a dependent thinning of the original point process where the thinning involves eNodes 3, 6, and 10 (this last interfering eNodeB was not shown in Figure 1(a)). Their Voronoï cells are colored in green.

resource blocks for a given eNodeB $i$ ($i > 0$) denoted $D_i$ is then given by

$$\mathbb{P}(D_i = k) = \pi_0 \frac{\rho^k}{k!}, \tag{3}$$

where $\pi_0 = \mathbb{P}(D_i = 0)$ and $RB_{max} \geq k \geq 0$.

These RB are allocated in a cyclic order. If the last $RB$ used by eNodeB $i-1$ has index $k$, eNodeB $i$ uses $RB$ indexed from $(k+1)\, mod(RB_{max})$ to $(k + D_i)\, mod(RB_{max})$.

For eNodeB 0, we do not consider the total number of allocated RB ($D_0$), but instead, a random variable $R_0$. It describes the index of the last RB used by eNodeB 0. Indeed, for this particular eNodeB, the quantity used in practice to compute the next allocation (RB indexes used by eNodeB 1) is $R_0$ rather than $D_0$. A formal definition of $R_0$ is given in appendix (Appendix A). An example of allocation is given in Figure 1.

The distribution of $R_0$ is set according to the stationary distribution of a Markov chain. The transition probabilities of this Markov chain are

$$P_{l,m} = \mathbb{P}(R_{n+1} = m \mid R_n = l) \tag{4}$$

$$= \sum_{j=0}^{+\infty} \sum_{u=max(0,m-l)}^{RB_{max}-l-1} \pi_0 \frac{\rho^{RB_{max}+m-u-l}}{(RB_{max}+m-u-l)} \pi_0^j \frac{(j\rho)^u}{u!}, \tag{5}$$

where $(l,m) \in \{0,1,..,RB_{max}-1\}^2$. The motivation for this particular construction is to keep the probability of using the resource 0 between eNodeB homogeneous. More precisely, it is built in order to verify the property given in Proposition 1. Details about the Markov chain construction are given in appendix (Appendix A). It is worth noting that other distributions for the resource demands (given by (3) in our case) can be considered as well. As soon as the distribution of $R_0$ verifies Proposition 1, the method proposed in this paper holds.

*3.4. Property of These Assignment Strategies.* We define more precisely the sequence of r.v. $(w_i)_{i\in\mathbb{N}}$. It indicates which eNodeB interferes with the typical user. It was already used in (1).

$$w_i = \begin{cases} 1, & \text{if eNodeB at } X_i \text{ uses RB with index 0} \\ 0, & \text{otherwise.} \end{cases} \tag{6}$$

By convention, we set $w_0 = 1$ a.s. In the following, we shall thus assume that $\mathbb{P}(w_i = 1 \mid w_0 = 1) = \mathbb{P}(w_i = 1)$.

**Proposition 1.** *For the three allocation strategies defined in Sections 3.1, 3.2, and 3.3, the following property holds:*

$$\mathbb{P}(w_j = 1 \mid w_i = 1) = \mathbb{P}(w_{j-i} = 1 \mid w_0 = 1) \tag{7}$$

The proofs for the first two strategies are straightforward. For the $M/M/RB_{max}/RB_{max}$ strategy, the distribution of $R_0$ has been set to verify this property (see Appendix A).

*3.5. Heuristics.* We compare these strategies to heuristics that aim to optimize interference or spatial reuse for a given configuration. It allows us to compare our RB assignment and performs in a cyclic manner around a typical user, to strategies where a controller in charge of a set of eNodeB will assign RB in order to optimize a certain objective function. For the heuristic minimizing the sum of interference, named "minimize interference" hereafter, the considered optimization problem is similar to the one developed in [3]. The problem has been shown NP-hard, so we use a greedy algorithm to find a solution. The number of users associated with each eNodeB follows the same distribution as the $M/M/RB_{max}/RB_{max}$ allocation. Then, we consider users in a random order and apply Algorithm 1 to associate an RB to a user. It chooses the resource block that minimizes the sum of interference. Obviously, we compute interference only

```
Data: RB_max: Total number of RB.
cost: sum of interference for the current allocation.
bestCost: sum of interference for the best allocation strategy, initialized to -1.
Result: Assign an RB to a user. This algorithm is called by the controller for each
        new user.
for each rb ∈ {0, 1, .., RB_max − 1} do
    if rb is free then
        assign rb to this user;
        cost ← sum_Interference();
        if bestCost <0 or cost<bestCost then
            Save this allocation strategy;
            bestCost = cost;
        end
    end
end
Assign the saved allocation strategy
```

Algorithm 1: Minimizing global interference.

for the users already assigned. The typical user is considered in last when the system has reached the targeted load. This algorithm mimics an assignment strategy where the RB are assigned at the arrival of the users request without changing the already assigned RB.

The second heuristic, "maximize reuse distance", maximizes the distance at which the RB are reused. Each user is considered in a random order. Different RB are assigned to the $RB_{max}$ first users. When assigning an RB to the other users, the controller chooses the RB for which the reuse distance is maximum. The typical user is considered in last. This second heuristic may correspond to a case where the controller does not have information on channel conditions and interference but knows the distances between eNodeB.

## 4. Interference Characterization

We derive the mean and the variance of interference for the three assignment strategies defined in the previous section.

The point process modeling interferers is a dependent thinning of the original PPP. Consequently, conditions for mean (respectively variance) to be finite with a PPP also hold for our point process: the path loss function $l(\cdot)$ must belong to $L^1$ (respectively, $L^2$).

*4.1. Distribution of Distances between the Typical User and eNodeB ($\|X_i\|$).* As a preamble, we give the PDF of the distance between the typical user at the origin and eNodeB. Both PDF of $\|X_i\|$ and joint distribution of $(\|X_i\|, \|X_j\|)$ are derived. These PDF are used in the computation of the mean and the variance of interference.

In the numerical evaluation, we shall condition interference by the distance $\|X_0\|$. It allows us to study interference for a given distance between the typical user and its attached eNodeB. It is also motivated by the computation of the SIR where both interference and the typical user signal strength depend on the distance $\|X_0\|$.

For our model, the PDF of $\|X_i\|$ with $i > 0$ given $\|X_0\| = r$ is

$$f^{i}_{\|X_0\|=r}(u, r) = \frac{(\lambda_e \pi)^i}{(i-1)!} 2u \left(u^2 - r^2\right)^{i-1} e^{-\lambda_e \pi (u^2 - r^2)} \mathbb{1}_{u>r} \quad (8)$$

The joint PDF of $(\|X_i\|, \|X_j\|)$ with $j > i > 0$ given $\|X_0\| = r$ is

$$\begin{aligned} f^{i,j}_{\|X_0\|=r}(u, v, r) &= \frac{(\lambda_e \pi)^j}{(i-1)!\,(j-i-1)!} 4uv \left(v^2 - u^2\right)^{j-i-1} \\ &\quad \times \left(u^2 - r^2\right)^{i-1} e^{-\lambda_e \pi (v^2 - r^2)} \mathbb{1}_{v>u>r} \end{aligned} \quad (9)$$

To obtain the PDF when $\|X_0\|$ is not set ($f_{\|X_i\|}(\cdot)$ and $f_{\|X_i\|,\|X_j\|}(\cdot)$), it suffices to integrate the two conditional PDF with regard to the PDF of $\|X_0\|$ given in (2).

*4.2. Mean of Interference.* The mean is derived from (1):

$$\begin{aligned} &\mathbb{E}\left[I\left(\|X_0\|\right)\right] \\ &\quad = \mathbb{E}\left[h_1\right] \sum_{i=1}^{+\infty} \mathbb{E}\left[w_i\right] \mathbb{E}\left[T_x\left(\|X_i - U_i\|\right) \cdot l\left(\|X_i\|\right)\right] \end{aligned} \quad (10)$$

In this equation, $w_i$ has been separated from the expectation as it is independent of the process $N_e$ (according to the defined strategies). We derive $\mathbb{E}[T_x(\|X_i - U_i\|) \cdot l(\|X_i\|)]$ and $\mathbb{E}[w_i]$ in the two next sections.

*4.2.1. Computation of $\mathbb{E}[T_x(\|X_i - U_i\|) \cdot l(\|X_i\|)]$*

*No Power Control.* In absence of power control, i.e., when $T_x(\cdot)$ is constant or independent of the process $N_e$, a closed formula may be expressed for (10). $\mathbb{E}[T_x(\|X_i - U_i\|) \cdot l(\|X_i\|)]$

is then given by $\mathbb{E}[T_x]\mathbb{E}[l(\|X_i\|)]$. Expectation of $l(\|X_i\|)$ is obtained from the distribution of $\|X_i\|$ given in Section 4.1.

$$\begin{aligned}&\mathbb{E}\left[I\left(\|X_0\|\right)\right]\\&\quad=\mathbb{E}\left[h_1\right]\sum_{i=1}^{+\infty}\mathbb{E}\left[w_i\right]\mathbb{E}\left[T_x\left(\|X_i-U_i\|\right)\right]\mathbb{E}\left[l\left(\|X_i\|\right)\right]\end{aligned}\tag{11}$$

*Power Control.* When the transmission power depends on the distance between the receiver and its attached eNodeB ($T_x(\|X_i - U_i\|)$), the computations are more complex. $E[T_x(\|X_i - U_i\|) \cdot l(\|X_i\|)]$ cannot be approximated by $\mathbb{E}[T_x(\|X_i-U_i\|)]E[l(\|X_i\|)]$ as the size of the Voronoï cell with nucleus $X_i$ depends on its distance to the origin. The joint distribution of $(\|X_i\|, \|X_i - U_i\|)$ being unknown, we propose the following approximation:

$$f_{\|X_i\|}(r)\, f^0_{\|U_i-X_i\|}(u,r)\tag{12}$$

with

$$f^0_{\|U_i-X_i\|}\left(u,\|X_i\|\right)=2\pi\lambda_e c_i\left(\|X_i\|\right)ue^{-\lambda_e c_i(\|X_i\|)\pi u^2}\tag{13}$$

The PDF of $\|U_i - X_i\|$ is the same as $\|U_0 - X_0\|$ given by (2). Its parameter $c_i(\|X_i\|)$ depends on $\|X_i\|$: $c_i(\|X_i\|) = 1/4\sqrt{\lambda_e}(\gamma_i\|X_i\| + b)$ with $\gamma_i = (1/2 - b)/\mathbb{E}[\|X_i\|]$ and $b = 0.33$. The motivation and the computation details for this PDF are given in appendix (Appendix B). We obtain

$$\begin{aligned}&\mathbb{E}\left[T_x\left(\|X_i-U_i\|\right)\cdot l\left(\|X_i\|\right)\right]\\&\quad=\int_0^{+\infty}T_x(u)\,l(r)\,f_{\|X_i\|}(r)\,f^0_{\|U_i-X_i\|}(u,r)\,du\,dr.\end{aligned}\tag{14}$$

Often, in real systems, the transmission power cannot be set arbitrarily and is limited to a set of predetermined values. The transmission power function can then be represented as a step function, $T_x(r) = \sum_{i=1}^{N_T} t_i \mathbb{1}_{r\in[\alpha_{i-1},\alpha_i]}$ where $N_T$ is the number of possible transmission powers, $t_i$ the $i^{th}$ transmission power value, and $[\alpha_{i-1}, \alpha_i]$ the distance interval between a user and its eNodeB at which this transmission power is used. An example of such setting is given in the numerical evaluation section. In this case, (14) becomes

$$\begin{aligned}&\mathbb{E}\left[T_x\left(\|X_i-U_i\|\right)l\left(\|X_i\|\right)\right]\\&\quad=\sum_{i=1}^{N_T}t_j\int_0^{+\infty}\left(e^{-\lambda_e c_i(r)\pi\alpha_j^2}-e^{-\lambda_e c_i(r)\pi\alpha_{j-1}^2}\right)f_{\|X_i\|}(r)\,dr\end{aligned}\tag{15}$$

When the computation is performed for a given distance $\|X_0\|$, the PDF $f_{\|X_i\|}(\cdot)$ in (12) and (15) must be replaced by $f^i_{\|X_0\|=r}(\cdot,\cdot)$ (given in Section 4.1).

*4.2.2. Computation of* $\mathbb{E}[w_i]$. Finally, in order to compute (10), we need to express $\mathbb{E}[w_i]$. First, note that $\mathbb{E}[w_i] = \mathbb{P}(w_i = 1)$.

**Proposition 2.** *The probability for eNodeB i to interfere with the typical user is given by*

(i) *Independent allocation*

$$\mathbb{P}\left(w_i=1\right)=\frac{1}{\Delta}\tag{16}$$

(ii) *Static allocation*

$$\mathbb{P}\left(w_i=1\right)=\mathbb{1}_{i\cdot mod(\Delta)=0}\tag{17}$$

(iii) $M/M/RB_{max}/RB_{max}$ *allocation*

$$\begin{aligned}\mathbb{P}\left(w_i=1\right)&=\pi_0^i\sum_{u=0}^{RB_{max}-1}\mathbb{P}\left(R_0=u\right)\\&\times\sum_{p=0}^{i\cdot RB_{max}-1-u}\frac{\left(\rho\left(i-1\right)\right)^p}{p!}\sum_{l=\lfloor(p+u)/RB_{max}+1\rfloor\cdot RB_{max}-(p+u)}^{RB_{max}}\frac{\rho^l}{l!}\end{aligned}\tag{18}$$

The computation details for the $M/M/RB_{max}/RB_{max}$ allocation are given in appendix (Appendix C).

*4.3. Variance of Interference.* Variance of interference is defined as

$$\mathbb{V}\left(I\left(\|X_0\|\right)\right)=\mathbb{E}\left[I\left(\|X_0\|\right)^2\right]-\mathbb{E}\left[I\left(\|X_0\|\right)\right]^2.\tag{19}$$

For the second moment, we obtain

$$\begin{aligned}\mathbb{E}\left[I\left(\|X_0\|\right)^2\right]&=\mathbb{E}\left[h_1^2\right]\sum_{i=1}^{+\infty}\mathbb{E}\left[T_x\left(\|U_i-X_i\|\right)^2\right.\\&\quad\left.\cdot\, l\left(\|X_i\|\right)^2\right]\mathbb{P}\left(w_i=1\right)+2E\left[h_1\right]^2\\&\quad\cdot\sum_{1\le i<j<+\infty}\mathbb{E}\left[T_x\left(\|U_i-X_i\|\right)T_x\left(\|U_j-X_j\|\right)\right.\\&\quad\left.\cdot\, l\left(\|X_i\|\right)l\left(\|X_j\|\right)\right]\mathbb{E}\left[w_iw_j\right].\end{aligned}\tag{20}$$

As for the mean, complexity lies in the correlation between $\|X_i\|$ and $\|U_i - X_i\|$. The term $\mathbb{E}[T_x(\|U_i - X_i\|)^2 \cdot l(\|X_i\|)^2]$ is computed with the same method as the first moment.

*Computation of* $\mathbb{E}[T_x(\|U_i-X_i\|)T_x(\|U_j-X_j\|)l(\|X_i\|)l(\|X_j\|)]$. As $\|U_i - X_i\|$ (respectively, $\|U_j - X_j\|$) depends on $\|X_i\|$ (respectively $\|X_j\|$), we condition by the distribution of $(\|X_i\|, \|X_j\|)$ given in Section 4.1. Given $X_i$ and $X_j$, we use the same PDF as in (B.1) assuming that $\|U_i - X_i\|$ and $\|U_j - X_j\|$ are independent. The considered joint distribution of $(\|X_i\|, \|X_j\|, \|U_i - X_i\|, \|U_j - X_j\|)$ becomes

$$f^0_{\|U_i-X_i\|}(u,r)\,f^0_{\|U_j-X_j\|}(v,s)\,f_{\|X_i\|,\|X_j\|}(r,s).\tag{21}$$

When the distance $\|X_0\|$ is fixed, $f_{\|X_i\|,\|X_j\|}(\cdot,\cdot)$ must be replaced by the PDF $f^{i,j}_{\|X_0\|=r}(\cdot,\cdot,\cdot)$ given in Section 4.1.

*Computation of* $\mathbb{E}[w_iw_j]$. It has been shown that the sequence $(w_i)_{i>0}$ verifies (7) for the three strategies. It allows us to express $\mathbb{E}[w_iw_j]$ with $i > j$ as

$$\mathbb{E}\left[w_iw_j\right]=\mathbb{P}\left(w_{i-j}=1\right)\mathbb{P}\left(w_j=1\right).\tag{22}$$

**Proposition 3.** *The joint probability for two eNodeB i and j ($j > i$) to interfere with the typical user is given by*

(i) *Independent allocation*

$$\mathbb{E}\left[w_i w_j\right] = \frac{1}{\Delta^2} \tag{23}$$

(ii) *Static allocation*

$$\mathbb{E}\left[w_i w_j\right] = \mathbb{1}_{i \cdot mod(\Delta)=0; j \cdot mod(\Delta)=0} \tag{24}$$

(iii) $M/M/RB_{max}/RB_{max}$ *allocation*

$$\mathbb{E}\left[w_i w_j\right] = \mathbb{P}\left(w_{j-i} = 1\right)\mathbb{P}\left(w_i = 1\right) \tag{25}$$

*where* $\mathbb{P}(w_{\cdot} = 1)$ *is given by (18).*

## 5. Signal over Interference Ratio (SIR)

In our model, there is a strong correlation between the interfering eNodeB. It is generated by the allocation strategies and cannot be neglected. Also, a correlation exists between the location of an eNodeB and the size of its Voronoï cell. Consequently, classical approach based on PPP which uses Laplacian transform for instance cannot be applied here and a formal derivation of interference distribution seems intractable.

Nevertheless, the different simulations presented in the next section will show that the PDF of interference can be approximated by a log-normal distribution. The parameters of this distribution, mean and variance denoted by $m_{I_{dB}}(\cdot)$ and $\sigma_{I_{dB}}(\cdot)$, are directly derived from the previous analytical computations. The classical mapping between log-normal and normal parameters can be applied to derive parameters of the normal distribution when interferences are expressed in decibel. In the following, a variable is indexed by $dB$ when it is expressed in decibel.

We get

$$\begin{aligned}\mathbb{P}\left(SIR_{dB} \le \beta_{dB}\right) &= \mathbb{P}\left(10 \cdot \log_{10}\left(P_t\left(\|X_0\|\right) h_0 l\left(\|X_0\|\right)\right) - I_{dB}\left(\|X_0\|\right) \le \beta_{dB}\right) \\ &= \mathbb{P}\left(I_{dB}\left(\|X_0\|\right) \ge -\beta_{dB} + 10 \cdot \log_{10}\left(P_t\left(\|X_0\|\right) h_0 l\left(\|X_0\|\right)\right)\right)\end{aligned} \tag{26, 27}$$

Assuming that $I_{dB}(\|X_0\|)$ is normally distributed with mean $m_{I_{dB}}(\|X_0\|)$ and variance $\sigma_{I_{dB}}(\|X_0\|)$, we obtain

$$\mathbb{P}\left(SIR_{dB} \le \beta_{dB}\right) = \frac{1}{2}\left(1 - \mathbb{E}\left[erf\left(\frac{-\beta_{dB} + 10 \cdot \log_{10}\left(P_t\left(\|X_0\|\right) h_0 l\left(\|X_0\|\right)\right) - m_{I_{dB}}\left(\|X_0\|\right)}{\sqrt{2}\sigma_{I_{dB}}\left(\|X_0\|\right)}\right)\right]\right) \tag{28}$$

$$= \frac{1}{2}\left(1 - \int_0^{+\infty} erf\left(\frac{-\beta_{dB} + 10 \cdot \log_{10}\left(P_t(r)\, l(r)\right) - m_{I_{dB}}(r)}{\sqrt{2}\sigma_{I_{dB}}(r)}\right) f_{\|X_0\|}(r)\, dr\right) \tag{29}$$

When $h_0$ is not constant, the expectation with regard to its distribution must be taken into account in (28). In (29), $h_0$ is assumed to be constant that equals to 1. In these two equations, $erf(\cdot)$ is the error function.

## 6. Numerical Results

We consider an E-UTRA channel with a bandwidth of 5MHz with $RB_{max} = 15$ [33]. The path loss function is the same as [3]. It is expressed in dB: $l(r) = -128.1 - 37.6 \cdot \log_{10}(r)$ where $r$ is the distance (in km). $T_x(\cdot)$ is set in such a way to guarantee to each user a minimum receiving power. We set the transmission power function $T_x(\cdot)$ to ensure a signal power greater than or equal to $-72.4$ dBm at the reception as specified in [33]. For each 50 meters (from 50 to 500 meters), we compute the minimum transmitting power required to reach this threshold ($Tx(r) \cdot l(r) \ge -72.4$ dBm for each interval of 50 meters leading to 10 possible transmission powers). This step function models the case where eNodeB has a finite set of predetermined power. The process intensity modeling eNodeB is equal to 2.25 per km$^2$. It corresponds to the intensity of base stations in Paris (https://www.antennesmobiles.fr/). Random variables $h_i$ are supposed constant equal to 1. This assumption facilitates interpretation of the results but any distribution can be considered as well. It simply adds a factor in terms of variance (cf. (20)). We simulate the different strategies through a simulator coded in C available here (http://www.anthonybusson.fr/index.php/publications). In all simulations and numerical results we consider 50 eNodeB. The different sums in the equations (e.g., (10) and (20)) are then limited to 50. For each set of parameters, simulations have be run from 10,000 to several millions times depending on the evaluated quantities. The number of simulations/samples has been set in order to have negligible confidence intervals. They are consequently not shown in the different figures.

*Mean and Variance of Interference.* In Figure 2, we plot the mean and the standard deviation of interference obtained from simulations and computed from formulas (10), (19), and (20) when the distance $\|X_0\|$ varies. The theoretical evaluation closely matches empirical estimators obtained by simulations. As expected, the highest interference level is observed for the independent allocation, and the lowest level for the static allocation. The static and the $M/M/RB_{max}/RB_{max}$ allocations offer equivalent results with a multiplication factor

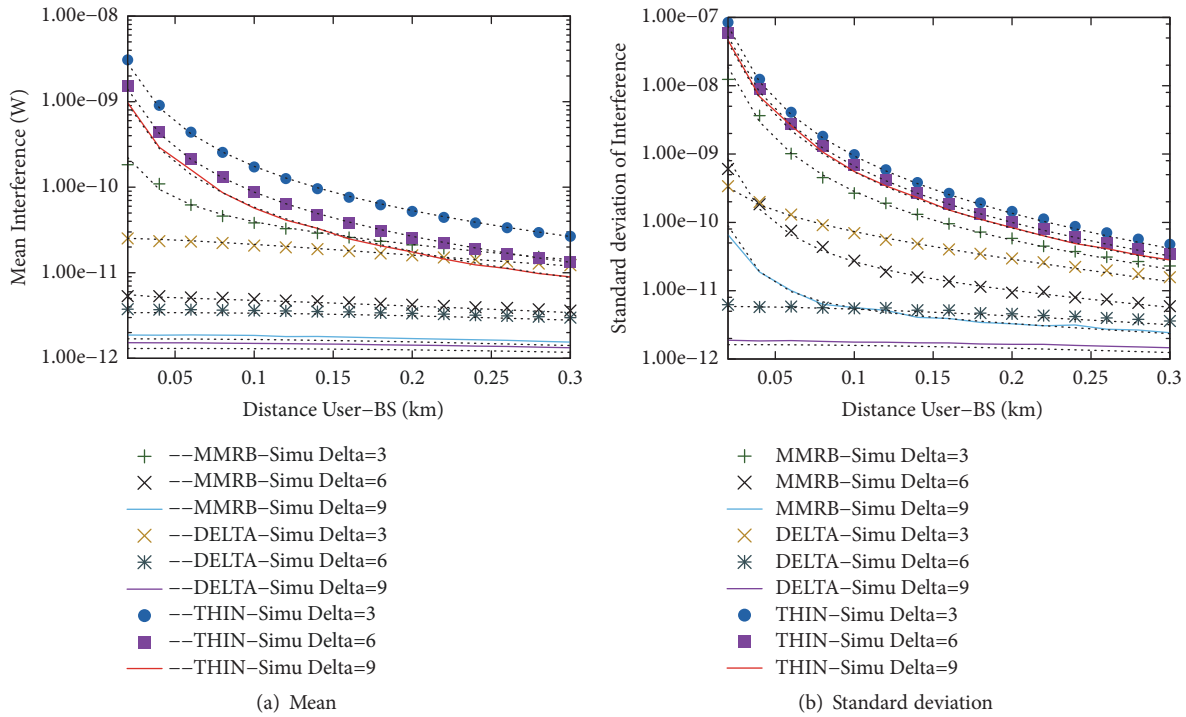


Figure 2: Interference: mean and standard deviation as a function of the distance between the typical user and its eNodeB ($\|X_0\|$). Simulation results are given by points and solid lines, and theoretical evaluations by the dotted lines.

Table 2: Mean and standarddeviation for the $M/M/RB_{max}/RB_{max}$ allocation and the two heuristics.

| Assignment strategy | $\Delta = 3$ | | $\Delta = 6$ | | $\Delta = 9$ | |
|---|---|---|---|---|---|---|
| | mean | std-dev | mean | std-dev | mean | std-dev |
| $M/M/RB_{max}/RB_{max}$ | $1.78e-11$ | $8.61e-11$ | $3.66e-12$ | $7.50e-12$ | $1.55e-12$ | $3.16e-12$ |
| Minimize Interference | $9.94e-12$ | $3.07e-11$ | $1.86e-12$ | $1.88e-12$ | $7.56e-13$ | $6.26e-13$ |
| Maximize reuse distance | $5.26e-11$ | $7.51e-10$ | $1.18e-11$ | $1.07e-10$ | $2.58e-12$ | $1.09e-11$ |

varying from 1.1 to 8.7 for the mean interference. Instead, the independent allocation differs deeply. Mean and standard deviation are multiplied by a factor ranging from 1.7 to 700 for the mean and can reach up to $2.6 \times 10^4$ for the standard deviation (for $\|X_0\| = 0.02$ km). The use of the thinned point process is thus questionable to approximate realistic assignment strategies. This strategy is no more considered in the following.

*Extrapolation of Interference Distribution.* We compare empirical distributions obtained from simulations to known distributions for the different strategies and the two heuristics when $\Delta = 3$, 6, and 9. Three of these empirical distributions are shown in Figure 3 (in dB). The distribution parameters have been set according to the maximum likelihood. The distributions that best fit simulations vary according to the allocation strategy and the reuse factor $\Delta$. For 4 cases over 12, the distribution minimizing error is the normal distribution. As soon as an asymmetry is observed, other distributions are more accurate: log-normal, Weibull, and Inverse Gamma. We perform two hypothesis tests, T-test and Smirnov-Kolmogorov, for all these scenarios. The alternative hypothesis is systematically ruled out. For the $M/M/RB_{max}/RB_{max}$ strategy, best fits are given by the normal ($\Delta = 3$ and 6) and Weibull distributions ($\Delta = 9$).

Nevertheless, as mentioned in Section 5, when estimating the SIR distribution for the $M/M/RB_{max}/RB_{max}$ strategy, we use the normal law to model interference. Indeed, even if this distribution is not systematically the most accurate, it offers a good approximation as shown in Figure 4 where the empirical and normal CDF are plotted. Moreover, simulations will show that this assumption does not impact the accuracy of the analytical model.

*Heuristics.* Simulations have shown that allocations resulting from the two heuristics correlate the transmission powers, the distance between eNodeB reusing the same resource, and the random variables $w_i$. When minimizing interference, correlations are caused by resource blocks allocated to users that require a low transmission power and that can be reused at a short distance and inversely. The transmission power is then correlated to $w_i$ and to the distance of eNodeB that reuse the same resource. These complex phenomena impede the proposal of an analytical model for these two heuristics. For comparison purposes, Table 2 reports mean and standard deviation for the two heuristics and the $M/M/RB_{max}/RB_{max}$

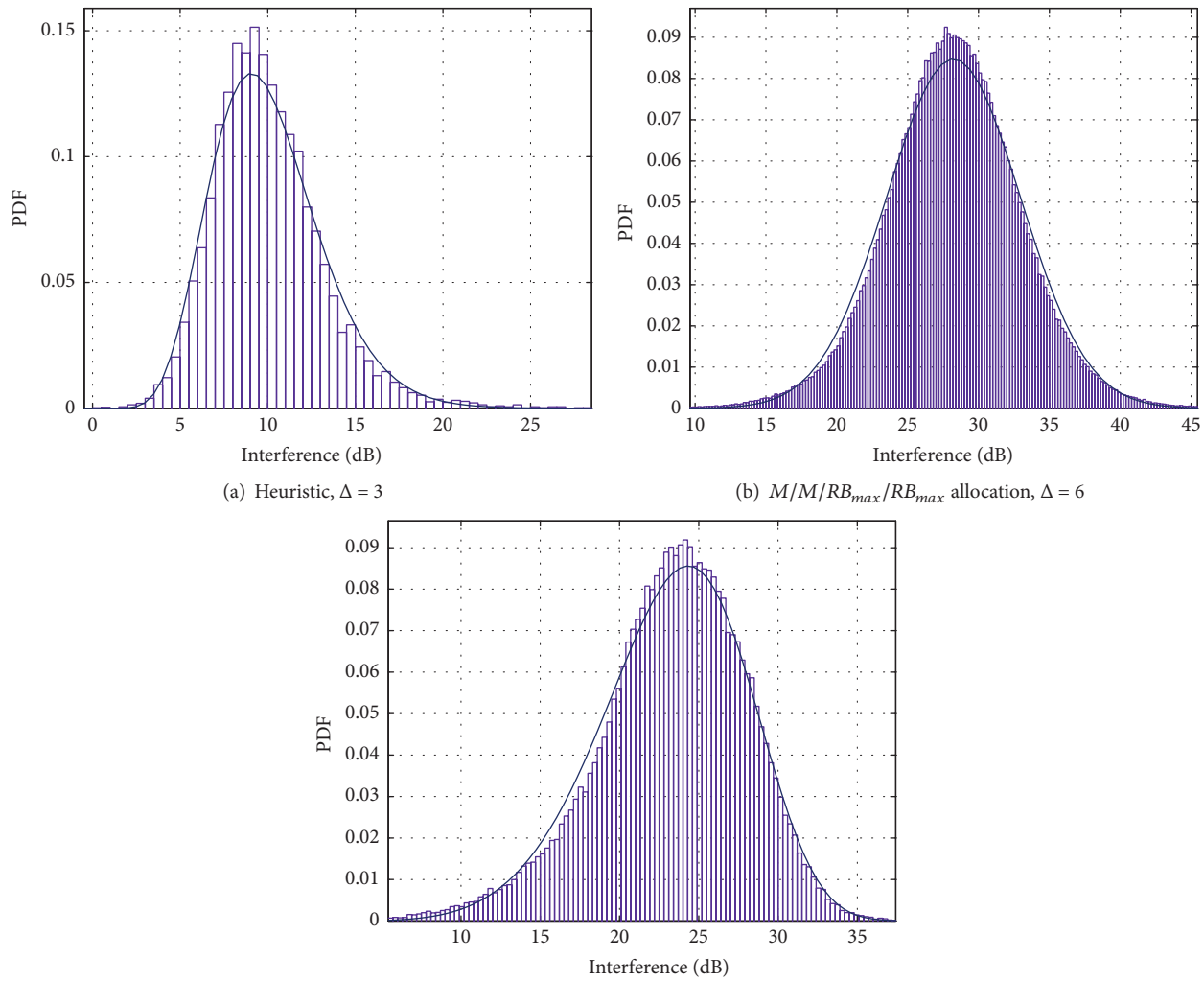


(a) Heuristic, $\Delta = 3$

(b) $M/M/RB_{max}/RB_{max}$ allocation, $\Delta = 6$

(c) Static allocation, $\Delta = 9$

Figure 3: Interference distribution: empirical (histogram) and extrapolation (curve). Among the classical distributions, the best extrapolations are Gamma (m=10.03, var=9.77), normal (m=28.23, var=22.16), and Weibull (a=25.14,b=5.75) for the heuristic, MMRB allocation $\Delta = 6$ and static allocation $\Delta = 9$, respectively.

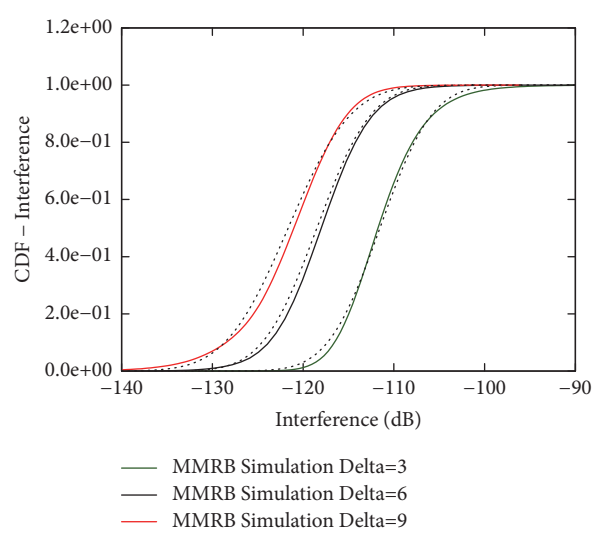


Figure 4: CDF of interference for the $M/M/RB_{max}/RB_{max}$ strategy. Empirical distributions are represented through the solid lines. CDF of the Normal distribution are plotted with dotted lines. Their parameters are obtained from the theoretical formulas. The $L^{+\infty}$ errors are $3.38e^{-02}$, $4.93e^{-02}$, and $5.65e^{-02}$ for $\Delta = 3$, 6, and 9, respectively.

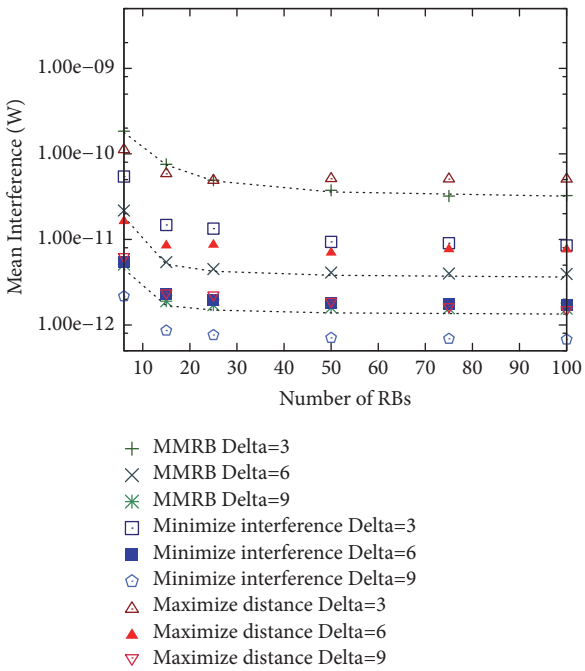


Figure 5: Mean interference when the number of RB varies. The load is adjusted to keep a constant reuse factor ($\Delta = 3$, 6, or 9). The distance $\|X_0\|$ is set to 50 meters. Dotted lines correspond to the theoretical evaluation of mean interference for the $M/M/RB_{max}/RB_{max}$ allocation and points to simulations.

allocation. The heuristic minimizing interference presents the best results. This difference was expected as the objective function minimizes interference and because the second heuristic maximizes the reuse distance without taking into account transmission powers. $M/M/RB_{max}/RB_{max}$ allocation offers interesting results with an intermediary interference level between the two heuristics. Even if interference is lower for the heuristic minimizing interference, its complexity in terms of feedback/measures from users and eNodeB is significantly greater than the other strategies. Indeed, it assumes that the scheduler knows, before an assignment, the interference contribution of each eNodeB on each user.

*Impact of the Number of RB.* We performed simulations and theoretical estimations of interference for different values of $RB_{max}$: 6, 15, 25, 50, 75, and 100 corresponding to different bandwidth of E-UTRA [33]. Results are shown in Figure 5 for the $M/M/RB_{max}/RB_{max}$ allocation and the two heuristics. The workload is adapted in order to keep the same $\Delta$ reuse factor. It appears that the mean interference is quite insensitive to the number of RB except when $RB_{max} = 6$. The impacting factor is thus the reuse factor $\Delta$ rather than the number of RB. Also, the same hierarchy between the three strategies is observed, except for $RB_{max} = 6$.

*SIR Distribution.* We evaluate the SIR CDF according to (29) for the $M/M/RB_{max}/RB_{max}$ allocation. This CDF is compared to the one obtained by simulations in Figure 6(a). We clearly observe that the analytical model offers very tight estimates of the SIR distribution. The assumption about the normal distribution of interference does not introduce a noticeable error. The SIR distribution for the $M/M/RB_{max}/RB_{max}$ strategy and the two heuristics are compared in Figure 6(b). The three CDF are similar and the $M/M/RB_{max}/RB_{max}$ allocation still offers an intermediate distribution between the two heuristics. The $L^{+\infty}$ norm between the three CDF is 0.192, 0.266, and 0.221 for $\Delta = 3$, 6, and 9, respectively.

*Modulation and Coding Rate.* The SIR distribution allows us to estimate modulations and coding rates that could be offered to users. We consider the thresholds between the required SIR and coding rate given in [33]. Applied to the SIR distribution, it gives the proportion of users that benefits from a certain modulation scheme and coding rate. The couple modulation/coding rate is referred to as transmission rate in the following. This proportion is given in Figure 7(a) for the $M/M/RB_{max}/RB_{max}$ allocation when the density of eNodeB increases from 2.25 (the default intensity considered in the previous evaluation) to 20 eNodeB per km$^2$. It appears that the network densification, even with a factor 10, does not significantly improve the transmission rate. Only the best transmission rate (64QAM-CR=4/5) really benefits from this densification with a proportion of users increasing from 3.5% to 11.6%.

The spatial reuse has much more impact on the transmission rates as it is shown in Figure 7(b). It clearly increases the transmission rates that are shifted from (QPSK CR=1/2-64QAM CR=2/3) for $\Delta = 3$ to (16QAM CR=1/2-64QAM CR=4/5) for $\Delta = 9$. The mean transmission rate increases almost of a factor 2 from 2.31 to 4.24 bits/baud.

Finally, we compare in Figure 7(c) the transmission rates for the three allocation strategies. As already observed in the previous plots, the heuristic minimizing interference offers better performance but is comparable to the two other strategies. For instance, for $\Delta = 6$, the mean transmission rates are close: 3.63, 3.23, and 3.92 bits/baud for the $M/M/RB_{max}/RB_{max}$ allocation, the heuristic maximizing the reuse distance, and the one minimizing interference respectively.

## 7. Conclusion

In recent LTE standards, a server may assign RB to a set of eNodeB to control resource usage and optimize performance in a global way. Even if it exists solutions to address this problem for a given configuration and topology, literature lacks models that evaluate performance of these RB allocations for a wide range of scenarios and at large scale.

To address this problem, we propound a spatial stochastic model that takes into account RB assignment strategies, realistic traffic demands, and power control. We propose analytical estimates for the two first moments of interference. This computation is based on two approximations: the distribution of the distance between a point uniformly distributed in a cell that models the user-eNodeB distance, and the joint distribution of the distances eNodeB-origin and user-eNodeB. For the latter, simulations have shown that these

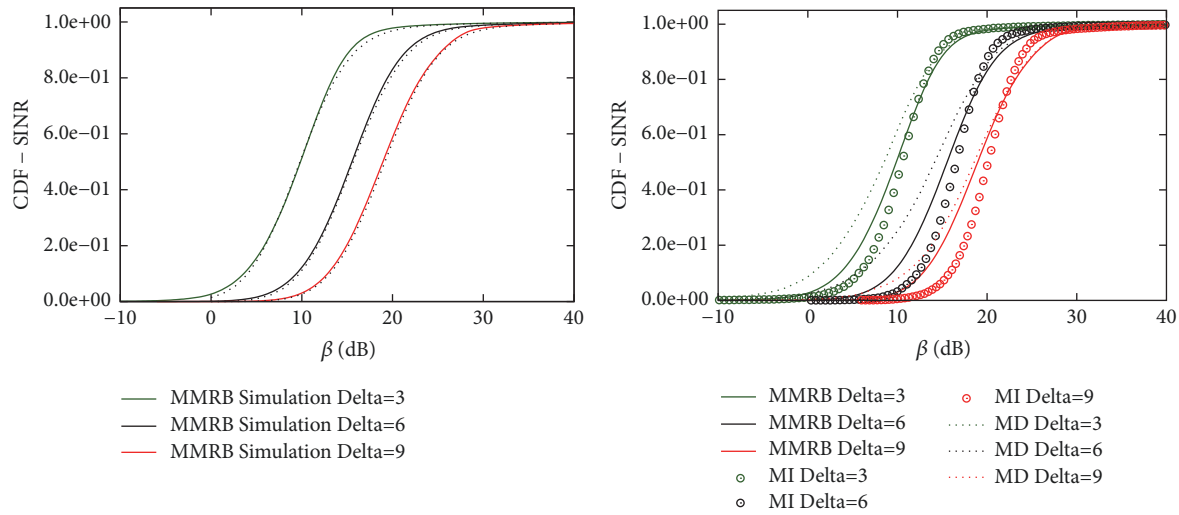


(a) SIR: empirical and theoretical CDF for the $M/M/RB_{max}/RB_{max}$ allocation

(b) SIR: empirical CDF for the three strategies. MI: maximize interference. MD: maximize distance

Figure 6: (a) We compare the distribution of SIR obtained by simulations (solid lines) and given by (29) (dotted lines). Errors with regard to the $L^{+\infty}$ norm are $2.47e-02$, $1.54e-02$, and $1.58e-02$ for $\Delta = 3$, 6, and 9 respectively. (b) CDF for the three allocation strategies ($M/M/RB_{max}/RB_{max}$ and Heuristics).

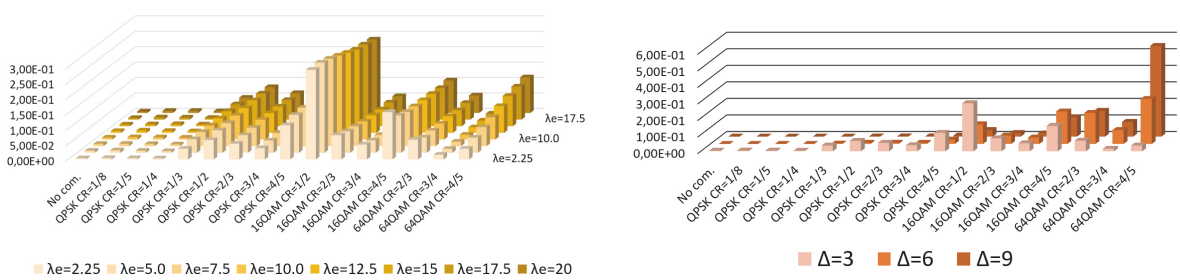


(a) $M/M/RB_{max}/RB_{max}$ allocation: $\lambda_e$ varies; $\Delta = 3$. CR=coding rate

(b) $M/M/RB_{max}/RB_{max}$ allocation: $\Delta = 3$, 6, and 9; $\lambda_e = 2.25$

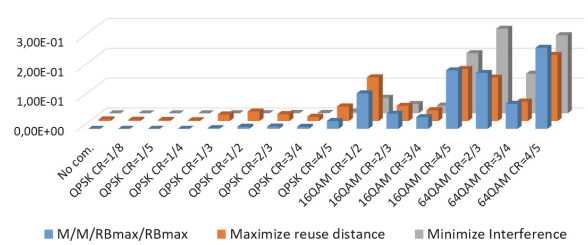


(c) $M/M/RB_{max}/RB_{max}$ and the two heuristics: $\Delta = 6$; $\lambda_e = 2.25$

Figure 7: Modulation and coding rate for the $M/M/RB_{max}/RB_{max}$ allocation strategy when the density of eNodeB increases (Figure 7(a)), for different reuse factor (Figure 7(b)), and comparison with the two heuristics (Figure 7(c)).

variables are strongly correlated, particularly for the points of the process close to the origin. This correlation impacts the transmission power used by the eNodeB and consequently interference and SIR distributions. The derivation of the SIR distribution allows us to express the classical outage but also the transmission rates in terms of modulation/coding rate that provide interesting insights on the throughput offers to the users. Also, it appears that eNodeB densification does not significantly improve the network performance in terms of throughput except for a small percentage of users for which the transmission rate is increased. Spatial reuse, expressed through the parameter $\Delta$ in our study, has a much more impact on the performance as the transmission rates are significantly increased. This spatial reuse must be expressed as the ratio between the total number of available resources over the number of users/requests per cell. Indeed, we have

observed that the system performance is quite insensitive to variation of these quantities when this ratio stays constant.

Beside, simulations show that the RB assignment strategies developed for the model give results close to the ones given by classical optimization problem which minimizes global interference or maximizes spatial reuse distances. It empirically shows that our analytical model is able to evaluate performance of classical optimization approaches but at large scale in terms of number of nodes, configurations, and topologies.

## Appendix

### A. Construction of the Markov Chain

In this section, we introduce the Markov chain used to set the distribution of $R_0$. We consider that the RB used between the typical user and its eNodeB has index $res$ ($res \in \{0, .., RB_{max} - 1\}$). We shall prove that this index does not impact calculation (we have chosen $res = 0$ in this paper by sack of simplicity).

We set the distribution of the number of used resource blocks at eNodeB 0 in such a way that it leads to the following property ($j > i \geq 0$):

$$\mathbb{P}\left(w_j = 1 \mid w_i = 1\right) = \mathbb{P}\left(w_{j-i} = 1 \mid w_0 = 1\right) \tag{A.1}$$

In order to obtain this property, we first introduce some preliminary notations and results. An example of allocation with the different notations is shown in Figure 1. We define a sequence of r.v. $(R_n)_{n\geq 0}$. If eNodeB $i$ is the $n^{th}$ eNodeB using $res$ and if $End_n$ is the index of the last RB used by this eNodeB then

$$R_n = \begin{cases} End_n - res & \text{if } End_n > res \\ End_n + RB_{max} - res & \text{otherwise.} \end{cases} \tag{A.2}$$

If eNodeB $i$ is the $n^{th}$ interfering eNodeB (using $res$), then eNodeB $j$ ($j > i$) is the $n + 1^{th}$ if and only if

$$R_n + \sum_{k=i+1}^{j-1} D_k < RB_{max} \tag{A.3}$$

and

$$R_n + \sum_{k=i+1}^{j} D_k \geq RB_{max} \tag{A.4}$$

In this case, $R_{n+1}$ is given by

$$R_{n+1} = R_n + \sum_{k=i+1}^{j} D_k - RB_{max} \tag{A.5}$$

As $(D_i)_{i>0}$ are i.i.d., the sequence $(R_n)_{n\geq 0}$ is a homogeneous Markov chain. The transition probabilities for $(l, m) \in \{0, 1, .., RB_{max} - 1\}^2$ are given by $P_{l,m} = \mathbb{P}(R_{n+1} = m \mid R_n = l)$.

The event $\{R_{n+1} = m\}$ given that $\{R_n = l\}$ occurs if and only if it exists $j \geq 0$ such that

$$\begin{aligned} R_n + \sum_{k=0}^{j} D_k &< RB_{max} \\ R_n + \sum_{k=0}^{j+1} D_k &= RB_{max} + m \end{aligned} \tag{A.6}$$

We condition by the possible values of $\sum_{k=0}^{j} D_k$. Note that $\mathbb{P}(\sum_{k=0}^{j} D_k) = \pi_0^j((j\rho)^u/u!)$.

$$\begin{aligned} P_{l,m} = \sum_{j=0}^{+\infty} \mathbb{P}\Bigg( & R_n + \sum_{k=0}^{j} D_k < RB_{max}, R_n + \sum_{k=0}^{j+1} D_k \\ & = RB_{max} + m \mid R_n = l \Bigg) \end{aligned} \tag{A.7}$$

$$\begin{aligned} = \sum_{j=0}^{+\infty} \sum_{u=0}^{j\cdot RB_{max}} \mathbb{P}\Big( & R_n + u < RB_{max}, R_n + u + D_{j+1} \\ & = RB_{max} + m \mid R_n = l \Big) \mathbb{P}\left(\sum_{k=0}^{j} D_k = u\right) \end{aligned} \tag{A.8}$$

$$\begin{aligned} = \sum_{j=0}^{+\infty} \sum_{u=0}^{RB_{max}-l-1} & \mathbb{P}\left(D_{j+1} = RB_{max} + m - u - l\right) \\ & \cdot \mathbb{P}\left(\sum_{k=0}^{j} D_k = u\right) \end{aligned} \tag{A.9}$$

$$= \sum_{j=0}^{+\infty} \sum_{u=max(0,m-l)}^{RB_{max}-l-1} \pi_0 \frac{\rho^{RB_{max}+m-u-l}}{(RB_{max} + m - u - l)} \pi_0^j \frac{(j\rho)^u}{u!} \tag{A.10}$$

We set the distribution of $R_0$ with the corresponding stationary distribution. Consequently, the sequence $(R_n)_{n\geq 0}$ becomes identically distributed where $R_n$ follows the stationary distribution for all $n \geq 0$. Moreover, according to (A.3) and (A.4) the property given in (A.1) holds. Indeed, $R_n$, $\sum_{k=i+1}^{j-1} D_k$, and $\sum_{k=i+1}^{j} D_k$ have the same distribution as $R_0$, $\sum_{k=1}^{j-i-1} D_k$ and $\sum_{k=1}^{j-i} D_k$, respectively. In the model evaluation, the stationary distribution is obtained numerically from the transition probabilities. As soon as $R_0$ follows the stationary distribution, the index $res$ can be chosen arbitrarily.

### B. Conditional Distribution of $\|U_i - X_i\|$

Simulations have shown that, given $\|X_i\|$, the distribution of $\|X_i - U_i\|$ is still close to the one given by (2) but with a different parameter. So, we assume that the distribution of $\|X_i - U_i\|$ given $\|X_i\|$ is equal to (2) but with a parameter function of $\|X_i\|$ denoted $c(\|X_i\|)$:

$$f^0_{\|U_i - X_i\|}\left(u, \|X_i\|\right) = 2\pi\lambda_e c_i\left(\|X_i\|\right) u e^{-\lambda_e c_i(\|X_i\|)\pi u^2} \tag{B.1}$$

These simulations have also shown that $\mathbb{E}[\|X_i - U_i\| \mid \|X_i\| = r]$ may be approximated as an affine function: $a_i r + b_i$. We define $c_i(\cdot)$ accordingly. It leads to

$$c_i(r) = \frac{1}{4\lambda_e (a_i r + b_i)} \tag{B.2}$$

To set $a_i$ and $b_i$, we use the two following properties:

$$\mathbb{E}\left[\mathbb{E}\left[\|X_i - U_i\| \mid \|X_i\| = r\right]\right] = \mathbb{E}\left[\|X_i - U_i\|\right] \tag{B.3}$$

$$= \frac{1}{2\sqrt{\lambda_e}} \tag{B.4}$$

$$\mathbb{E}\left[\mathbb{E}\left[\|X_i - U_i\| \mid \|X_i\| = r\right]\right] = \mathbb{E}\left[a_i \|X_i\| + b_i\right] \tag{B.5}$$

$$= a_i \mathbb{E}\left[\|X_i\|\right] + b_i \tag{B.6}$$

Equation (B.4) is derived from (2), and (B.5) from our assumption on $c_i(r)$. $a_i$ is then set as a function of $b_i$, $\mathbb{E}[\|X_i\|]$, and $\lambda_e$. $b_i$ is obtained from our simulations. For a given intensity, $b_i$ has been observed almost constant with regard to $i$. The best approximation as a function of the intensity is given by $b_i = 0.33/\sqrt{\lambda_e}$. After a few manipulations, we obtain

$$c_i(r) = \frac{1}{4\sqrt{\lambda_e}(\gamma_i r + b)} \tag{B.7}$$

with $\gamma_i = (1/2 - b)/\mathbb{E}[\|X_i\|]$ and $b = 0.33$.

The joint distribution of $(\|X_i\|, \|U_i - X_i\|)$ is then approximated by

$$f_{\|X_i\|}(r)\, f^0_{\|U_i - X_i\|}(u, r) \tag{B.8}$$

## C. Proof of Proposition 2

First note that by convention we have $\mathbb{P}(w_i = 1) = \mathbb{P}(w_i = 1 \mid w_0 = 1)$. The event $\{w_i = 1\}$ occurs if and only if it exists $j \geq 1$ such that

$$\begin{aligned} R_0 + \sum_{k=1}^{i-1} D_k &< j \cdot RB_{max} \\ R_0 + \sum_{k=1}^{i} D_k &\geq j \cdot RB_{max} \end{aligned} \tag{C.1}$$

We get

$$\begin{aligned} \mathbb{P}(w_i = 1) = \sum_{j=1}^{i} \mathbb{P}\Bigg( & R_0 + \sum_{k=1}^{i-1} D_k < j \cdot RB_{max}, R_0 \\ & + \sum_{k=1}^{i} D_k \geq j \cdot RB_{max} \Bigg) \end{aligned} \tag{C.2}$$

We condition by the possible values of the r.v. $R_0$, $\sum_{k=1}^{i-1} D_k$, and $D_i$:

$$\mathbb{P}(w_i = 1) = \sum_{j=1}^{i} \sum_{u=0}^{RB_{max}-1} \sum_{p=0}^{(i-1)\cdot RB_{max}} \mathbb{P}\left(u + p < j \cdot RB_{max}, u + p + D_i \geq j \cdot RB_{max}\right) \mathbb{P}(R_0 = u)\, \mathbb{P}\left(\sum_{k=1}^{i-1} D_k = p\right) \tag{C.3}$$

$$= \sum_{j=1}^{i} \sum_{u=0}^{RB_{max}-1} \sum_{p=0}^{(i-1)\cdot RB_{max}} \sum_{l=0}^{RB_{max}} \mathbb{1}_{u+p<j\cdot RB_{max}} \mathbb{1}_{u+p+l\geq j\cdot RB_{max}} \mathbb{P}(R_0 = u)\, \mathbb{P}\left(\sum_{k=1}^{i-1} D_k = p\right) \mathbb{P}(D_i = l) \tag{C.4}$$

$\mathbb{1}_{\cdot}$ is the indicator function. We use the property below

$$\begin{aligned} & \sum_{j=1}^{i} \mathbb{1}_{u+p<j\cdot RB_{max}} \mathbb{1}_{u+p+l\geq j\cdot RB_{max}} \\ & \quad = \mathbb{1}_{u+p+l\geq \lfloor (u+p)/RB_{max}+1 \rfloor \cdot RB_{max}} \end{aligned} \tag{C.5}$$

to get

$$\begin{aligned} \mathbb{P}(w_i = 1) = \pi_0^i & \sum_{u=0}^{RB_{max}-1} \mathbb{P}(R_0 = u) \\ & \cdot \sum_{p=1}^{i\cdot RB_{max}-1-u} \frac{(\rho(i-1))^p}{p!} \sum_{l=\lfloor (p+u)/RB_{max}+1 \rfloor \cdot RB_{max}-(p+u)}^{RB_{max}} \frac{\rho^l}{l!} \end{aligned} \tag{C.6}$$

## Data Availability

There is no data used in this paper. Nevertheless, the code of our simulator is made available (the link is in the paper).

## Conflicts of Interest

The authors declare that they have no conflicts of interest.

## References


[1] "Requirements for further advancements for e-utra (lte-advanced). 3gpp technical specification ts 36.913, release 13," 2015. http://www.3gpp.org.

[2] A. S. Hamza, S. S. Khalifa, H. S. Hamza, and K. Elsayed, "A survey on inter-cell interference coordination techniques in ofdma-based cellular networks," *IEEE Communications Surveys & Tutorials*, vol. 15, no. 4, pp. 1642–1670, 2013.

[3] D. López-Pérez, Á. Ladányi, A. Jüttner, H. Rivano, and J. Zhang, "Optimization method for the joint allocation of modulation schemes, coding rates, resource blocks and power in self-organizing LTE networks," in *Proceedings of the IEEE INFOCOM 2011*, pp. 111–115, April 2011.

[4] A. Guo and M. Haenggi, "Spatial stochastic models and metrics for the structure of base stations in cellular networks," *IEEE*

*Transactions on Wireless Communications*, vol. 12, no. 11, pp. 5800–5812, 2013.

[5] C.-H. Lee, C.-Y. Shih, and Y.-S. Chen, "Stochastic geometry based models for modeling cellular networks in urban areas," *Wireless Networks*, vol. 19, no. 6, pp. 1063–1072, 2013.

[6] W. Lu and M. D. Renzo, "Stochastic geometry modeling of cellular networks: analysis, simulation and experimental validation," in *Proceedings of the 18th ACM International Conference on Modelling, Analysis and Simulation of Wireless and Mobile Systems (MSWiM '15)*, pp. 179–188, New York, NY, USA, November 2015.

[7] Y. L. Lee, T. C. Chuah, J. Loo, and A. Vinel, "Recent advances in radio resource management for heterogeneous LTE/LTE-A networks," *IEEE Communications Surveys & Tutorials*, vol. 16, no. 4, pp. 2142–2180, 2014.

[8] F. Mhiri, K. Sethom, and R. Bouallegue, "A survey on interference management techniques in femtocell self-organizing networks," *Journal of Network and Computer Applications*, vol. 36, no. 1, pp. 58–65, 2013.

[9] X. Chen, L. Li, and X. Xiang, "Ant colony learning method for joint MCS and resource block allocation in LTE Femtocell downlink for multimedia applications with QoS guarantees," *Multimedia Tools and Applications*, vol. 76, no. 3, pp. 4035–4054, 2017.

[10] D. López-Pérez, X. Chu, A. V. Vasilakos, and H. Claussen, "On distributed and coordinated resource allocation for interference mitigation in self-organizing lte networks," *IEEE/ACM Transactions on Networking*, vol. 21, no. 4, pp. 1145–1158, 2013.

[11] H. Zhang, H. Liu, J. Cheng, and V. C. M. Leung, "Downlink energy efficiency of power allocation and wireless backhaul bandwidth allocation in heterogeneous small cell networks," *IEEE Transactions on Communications*, no. 99, 2017.

[12] H. Zhang, W. Zheng, X. Chu et al., "Joint subchannel and power allocation in interference-limited OFDMA femtocells with heterogeneous QoS guarantee," in *Proceedings of the IEEE Global Communications Conference (GLOBECOM '12)*, pp. 4572–4577, December 2012.

[13] H. Elsawy, E. Hossain, and M. Haenggi, "Stochastic geometry for modeling, analysis, and design of multi-tier and cognitive cellular wireless networks: a survey," *IEEE Communications Surveys & Tutorials*, vol. 15, no. 3, pp. 996–1019, 2013.

[14] H. ElSawy, A. Sultan-Salem, M.-S. Alouini, and M. Z. Win, "Modeling and analysis of cellular networks using stochastic geometry: a tutorial," *IEEE Communications Surveys & Tutorials*, vol. 19, no. 1, pp. 167–203, 2017.

[15] R. Kwan and C. Leung, "A survey of scheduling and interference mitigation in lte," *Journal of Electrical and Computer Engineering—Special Issue on LTE/LTE-Advanced Cellular Communication Networks*, pp. 1:1–1:10, 2010.

[16] J. G. Andrews, F. Baccelli, and R. K. Ganti, "A tractable approach to coverage and rate in cellular networks," *IEEE Transactions on Communications*, vol. 59, no. 11, pp. 3122–3134, 2011.

[17] T. D. Novlan, R. K. Ganti, A. Ghosh, and J. G. Andrews, "Analytical evaluation of fractional frequency reuse for OFDMA cellular networks," *IEEE Transactions on Wireless Communications*, vol. 10, no. 12, pp. 4294–4305, 2011.

[18] T. D. Novlan, R. K. Ganti, A. Ghosh, and J. G. Andrews, "Analytical evaluation of fractional frequency reuse for heterogeneous cellular networks," *IEEE Transactions on Communications*, vol. 60, no. 7, pp. 2029–2039, 2012.

[19] H. Zhuang and T. Ohtsuki, "A model based on poisson point process for downlink K tiers fractional frequency reuse heterogeneous networks," *Physical Communication*, vol. 13, pp. 3–12, 2014, Special Issue on Heterogeneous and Small Cell Networks.

[20] A. A. Gebremariam, T. Bao, D. Siracusa, T. Rasheed, F. Granelli, and L. Goratti, "Dynamic strict fractional frequency reuse for software-defined 5G networks," in *Proceedings of the IEEE International Conference on Communications (ICC '16)*, pp. 1–6, May 2016.

[21] N. Lee, D. Morales-Jimenez, A. Lozano, and R. W. Heath, "Spectral efficiency of dynamic coordinated beamforming: a stochastic geometry approach," *IEEE Transactions on Wireless Communications*, vol. 14, no. 1, pp. 230–241, 2015.

[22] X. Zhang and M. Haenggi, "A Stochastic geometry analysis of inter-cell interference coordination and intra-cell diversity," *IEEE Transactions on Wireless Communications*, vol. 13, no. 12, pp. 6655–6669, 2014.

[23] F. Baccelli and A. Giovanidis, "A stochastic geometry framework for analyzing pairwise-cooperative cellular networks," *IEEE Transactions on Wireless Communications*, vol. 14, no. 2, pp. 794–808, 2015.

[24] J. Yoon and G. Hwang, "Distance-based inter-cell interference coordination in small cell networks: stochastic geometry modeling and analysis," *IEEE Transactions on Wireless Communications*, 2018.

[25] B. Błaszczyszyn, M. Jovanovicy, and M. K. Karray, "How user throughput depends on the traffic demand in large cellular networks," in *Proceedings of the 12th International Symposium on Modeling and Optimization in Mobile, Ad Hoc, and Wireless Networks (WiOpt '14)*, pp. 611–619, May 2014.

[26] H. H. Yang and T. Q. S. Quek, "SIR coverage analysis in cellular networks with temporal traffic: a stochastic geometry approach," *Corrossion*, 2018.

[27] S. M. Yu and S.-L. Kim, "Downlink capacity and base station density in cellular networks," in *Proceedings of the 11th International Symposium and Workshops on Modeling and Optimization in Mobile, Ad Hoc and Wireless Networks (WiOpt '13)*, pp. 119–124, May 2013.

[28] Y. Wang, M. Haenggi, and Z. Tan, "The meta distribution of the sir for cellular networks with power control," *Corrossion*, 2017.

[29] M. S. Omar, S. A. Hassan, H. Pervaiz et al., "Multi-objective optimization in 5g hybrid networks," *IEEE Internet of Things Journal*, 2018.

[30] Y. Leo, A. Busson, C. Sarraute, and E. Fleury, "Call detail records to characterize usages and mobility events of phone users," *Computer Communications*, vol. 95, pp. 43–53, 2016.

[31] I. L. Cherif, *Spectral and Energy Efficiency in 5G Wireless Networks [Ph.D. thesis]*, Univeristy Paris Saclay, 2016.

[32] S. Mukherjee, *Analytical Modeling of Heterogeneous Cellular Networks. Analytical Modeling of Heterogeneous Cellular Networks: Geometry, Coverage, and Capacity*, Cambridge University Press, 2014.

[33] "Technical specification group radio access network; base station (bs) radio transmission and reception, 2012., Release 11.2; 3gpp ts 36.104 v11.2," 2012.